Optik - International Journal for Light and Electron Optics 229 (2021) 166290

Contents lists available at ScienceDirect

Optik

journal homepage: www.elsevier.com/locate/ijleo

Original research article

Thermal control of primary mirror of Space Solar Telescope

Shuang Yang [a,b], Changshuai Du [c], Xianwei Yang [a,*], Chunlong Liu [a,*], Yan Xiong [a,b], Richa Hu [a], Xusheng Zhang [a], Yong Huang [a], Liang Guo [a]

[a] Changchun Institute of Optics, Fine Mechanics and Physics, Chinese Academy of Sciences, Changchun, 130033, China
[b] University of Chinese Academy of Sciences, Beijing, 100049, China
[c] Technology and Engineering Center for Space Utilization, Chinese Academy of Sciences, Beijing, 100094, China

ARTICLE INFO

Keywords:
Lyman-alpha solar Telescope
Primary mirror
Graphite membrane
Thermal design
Finite element network
Thermal equilibrium test

ABSTRACT

The space-based Lyman-alpha Solar Telescope (LST) developed by China will conduct in-depth observation and research on solar activity and internal dynamics of the sun. Thermal control of the primary mirror is the core of the LST and ensures normal and efficient operation of the LST primary mirror. The primary mirror directly receives solar energy. Its element is produced from fused silica, and the multilayer coatings have high heat absorption. The primary mirror is connected with the front of the piezoelectric actuator for high-frequency image stabilization. According to these characteristics, we study the thermal properties of the primary mirror by attaching a high-thermal-conductivity graphite membrane to its back and connecting the annular bracket. We conduct a thermal equilibrium test and finite element network simulation in high-temperature mode, and their results differ by < 1 °C. High- and low-temperature simulations of the primary mirror in orbital operation show that it meets the thermal control target of < 40 °C. Therefore, applying a graphite membrane to the LST primary mirror well meets the needs of thermal control. This provides a theoretical basis for improving the reliability and thermal optimization of the primary mirror.

1. Introduction

The space solar telescope has played a vital role in observing and researching solar events such as coronal mass ejections (CMEs), solar flares, and sunspots. The space-based Lyman-alpha Solar Telescope (LST) developed by China has great practical significance for observing and studying the serious consequences of satellite breakdown, communication interruptions, geomagnetic storms, and harmful radiation on and around the Earth caused by solar activity. The overall structure of the LST is shown in Fig. 1. The primary mirror is the core window of the LST; it is the basic equipment for observing solar activity in the 121.6 nm and 700 nm bands and studying the internal dynamics of the sun. However, the cold black background, extreme low- and high-temperature transitions, single-particle effects, atomic oxygen corrosion, and other factors of the space environment can significantly affect observation. On the one hand, the LST primary mirror operates in a sun-synchronous orbit at a height of 720 km and will face a complex thermal environment including low-temperature space heat sinks, direct sunlight, infrared radiation from the Earth, and sunlight reflected from the Earth. On the other hand, there is a large difference between the heat flows on the sunny side and the shady side. This may lead to an uneven temperature distribution of the primary mirror, which affects the LST imaging quality. Therefore, it is necessary to ensure normal

* Corresponding authors.
E-mail addresses: yangxianwei521@163.com (X. Yang), 6033610432lcl@163.com (C. Liu).

https://doi.org/10.1016/j.ijleo.2021.166290
Received 27 November 2020; Accepted 7 January 2021
Available online 13 January 2021

operation of the LST primary mirror in orbit and reduce the influence of the thermal environment on the optical imaging quality. Accomplishing this requires designing a reliable, effective, and accurate thermal control system for the primary mirror.

The Solar Dynamics Observatory (SDO), launched by NASA in the United States in 2010, carried the Helioseismic and Magnetic Imager (HMI) to observe and study the interior dynamics of the sun. A 50 Å bandpass filter is set in front of the primary mirror, which reflects most of the direct solar energy, and the temperature is controlled in the range 28–35 °C. The primary mirror uses a passive thermal control method. A carbon fiber tube with a low thermal expansion coefficient is used between the primary mirror and the secondary mirror to reduce thermal deformation caused by the temperature conduction between these mirrors. The installation edge of the primary mirror is in contact with the outer tube wall, which directly radiates the heat of the primary mirror to the cold black background, thereby reducing the surface temperature and controlling the primary mirror temperature at about 20 °C [1,2].

The Solar Optical Telescope (Solar-B) launched by the United States and Japan in 2006 was equipped to observe the extreme ultraviolet band. A silver coating on the surface of the primary mirror minimizes solar energy absorption and increases the emissivity of the superficies of the primary mirror. The primary mirror absorbs 13–24 W of heat from the sun, and then the main mirror transmits the absorbed heat to the lower circular tube through the Invar support structure. Below the lower circular tube is the heat conduction and radiation plate, at the bottom of which is the bottom cooling plate consisting of gold-plated aluminum to absorb the back radiation of the primary mirror, thus keeping the temperature of the main mirror at 24 °C. The operating temperature of the primary mirror is always within the target temperature range after launch [3].

The Ultra-Compact Telescope observes the earth and space. It mainly observes the extreme ultraviolet band. The primary mirror of the EUV telescope is made of fused silica and has a target temperature of –40–(+60) °C, and the supporting structure is all made of Invar (with a linear expansion coefficient ~ 0.65e–6/°C). Therefore, the overall satellite frame is made of aluminum alloy to reduce the effect of thermal deformation caused by large temperature differences, and a thermally conductive aluminum plate is installed around the structure to radiate the heat of the primary mirror in time to the cold and black background [4].

The Solar Optical Telescope (Solar-C) launched by Japan in 2010 is equipped to observe extreme ultraviolet and near-infrared light. The surface of the primary mirror is coated with MgF_2, which reflects most of the energy of the sun and drops the temperature to below 50 °C. The primary mirror is supported by an Invar structure, which is connected to an aluminum cooling finger (emissivity $\varepsilon = 0.75$). The heat of the primary mirror can be transmitted to the cold finger through the Invar. The temperature of the primary mirror is controlled to be ~ 49 °C [5].

From the above, the primary mirror of the solar telescope is generally thermally controlled via passive control. The primary mirror is fixed on a support structure. Usually, a filter is set at the front end of the primary mirror to reflect most of the direct sunlight energy. And then, the primary mirror is connected to the surrounding main frame through the support structure, and the heat absorbed by the primary mirror is radiated to the cold black background via a radiating cold plate connected to the main frame, so that the temperature is controlled within the target range. However, the thermal control of the LST primary mirror studied in this paper is quite different from that of the above-mentioned space-based solar telescope in the following ways:

(1) The back of the primary mirror on the structure is connected with the front end of the piezoelectric actuator for high-frequency motion to stabilize the image, and the contact area of the supporting structure is very small, which is not conducive to heat dissipation.
(2) There is no filter at the front end of the primary mirror, which directly receives the solar radiation and observes two bands at the same time. The main mirror coating has a high solar absorption ratio and large heat absorption.
(3) The primary mirror material is fused silica, which has low thermal conductivity and an uneven temperature distribution.

Hence, this paper will study the thermal control of a high-thermal-conductivity graphite membrane for the primary mirror on the basis of the structural characteristics and thermal control difficulties described above. We use the thermal design of the primary mirror,

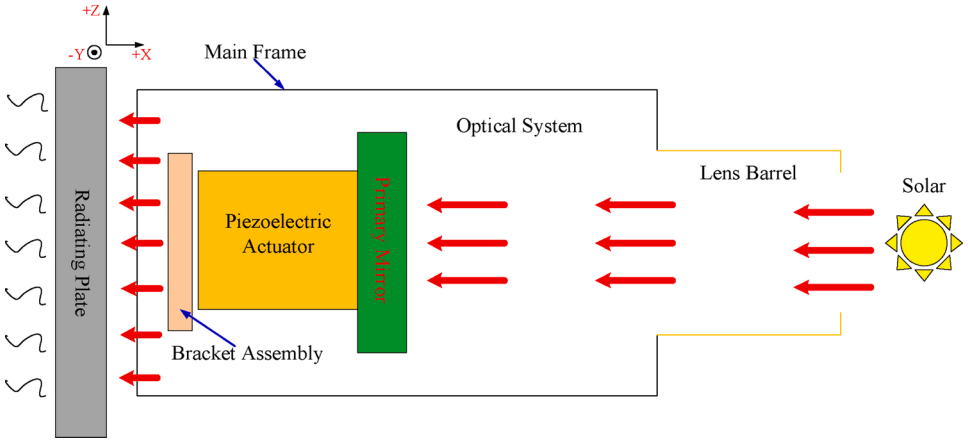

Fig. 1. Overall structure of Lyman-alpha Solar Telescope (LST).

a finite element network simulation, and a thermal equilibrium test to verify the extreme thermal properties of the graphite membrane. This is to ensure that the primary mirror of the LST meets the thermal control target.

2. Thermal design of the primary mirror

The LST Coronagraph uses an off-axis reflective optical system in which the primary mirror is used to observe the corona and heliosphere in the 121.6 nm and 700 nm bands simultaneously. Therefore, there is no filter at the front end of the primary mirror, and it directly receives the energy incident from the sun. The primary mirror material is fused silica, which has low thermal conductivity and an uneven temperature distribution. The primary mirror has a high solar absorption ratio and high heat absorption. The Ultra-Compact Telescope uses fused silica as the raw material of its main mirror. Its linear expansion coefficient (~ 0.54e–7/°C) is small and not easily affected by high temperature, which ensures normal imaging of the optical system [6,7]. Stray light is highly suppressed in the optical system because the primary mirror needs to observe both the corona and heliosphere of the sun, and the primary mirror needs to be efficiently and accurately oriented toward the sun in real time. Both the SDO and Solar-B use star sensors to adjust the attitude of the entire satellite to orient the primary mirror toward the sun. During this process, the energy consumption of the star sensors is high, the stability of solar orientation is low, and the image quality of the corona is poor [8]. Therefore, we studied the connection between the back of the LST primary mirror and the front of the piezoelectric actuator, which is designed to provide high-frequency motion to stabilize the image. The primary mirror was fine-tuned within a range of 20 μm to reduce the energy loss of the star sensors, ensure the quality of the coronal imaging, and improve the operational efficiency of the coronagraph. However, the back of the primary mirror and the front of the piezoelectric actuator are fixed at three points, and the contact area of the supporting structure is small, which is not conducive to the heat dissipation of the primary mirror. The Solar-B and Solar-C primary mirrors are each mounted on an aluminum alloy support frame. The outer area of the primary mirror is in contact with the aluminum alloy frame, which takes out heat from the mirror [3,9]. Hence, the annular bracket support of the LST primary mirror uses Invar to reduce the influence of thermal deformation caused by high heat absorption of the primary mirror structure. An aluminum bracket heat sink is installed at the rear of the piezoelectric actuator. Heat is transmitted to the frame in time, thus reducing the temperature of the primary mirror. Fig. 2 shows the specific structure of the primary mirror.

The LST runs in a 720 km sun-synchronous orbit with fixed sunny and shady sides, and is affected by the direct heat from the sun and the Earth's albedo and infrared radiation. The position of the satellite's radiating plate is determined by calculating the influence of the external heat flow on the satellite, and the design layout of the satellite's thermal control is reasonable. Fig. 3a shows the calculated high-temperature LST external heat flow, and Fig. 3b presents the low-temperature external heat flow. We see from the figure that the –X plane of the LST is least affected by external heat flow, which makes it suitable as the heat dissipation surface of the entire satellite. However, +X faces the sun with an external heat flow greater than 1400 W/m^2. There is no filter in front of the primary mirror, so its heat absorption is high because it directly receives intense solar radiation. During orbital operation, the sun's rays pass directly through the lens barrel to the primary mirror at an angle of 2″, and 4 W of energy enters the surface, so the surface temperature of the primary mirror is higher than 50 °C. This would directly affect imaging quality in long-term work while the primary mirror is oriented toward the sun. Therefore, effective thermal control of the primary mirror can ensure that the primary mirror operates normally and efficiently under dynamic image stabilization.

In this study, a thermally conductive graphite membrane (0.2 mm) is used to transfer the heat of the primary mirror to the frame to control the target temperature of the mirror to be less than 40 °C. When aggregates formed by highly graphitized isolated bubbles are combined with resin, the contact area increases, interface bonding strength is improved, heat transfer is greatly improved, and thermal conductivity reaches 1100 W/(m·K) [10–12]. The Moon Mineralogy Mapper-M3 launched by NASA in 2008 used an aluminum-encapsulated high-thermal-conductivity graphite membrane on the radiator and the side wall of the frame. Because the

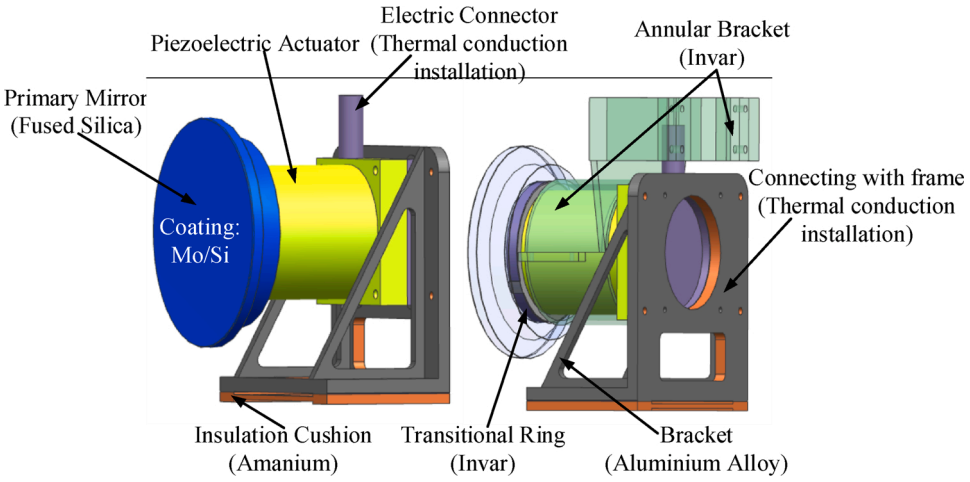

Fig. 2. Diagram of specific structure of LST primary mirror.

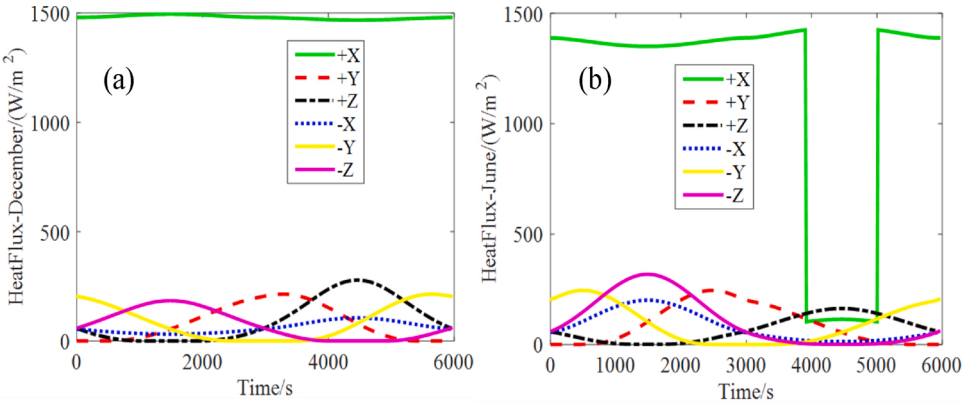

Fig. 3. Calculated external heat flow of LST.

thermal conductivity of the membrane reached 460 W/(m·K), heat could be conducted through it quickly to the radiator and then be radiated to the cold black background by the radiator [13–16]. In short-term high-power devices and periodic devices, the temperature is higher than 50 °C and the copper shell is used to encapsulate high-thermal-conductivity graphite. This consists of a phase-change thermal sink for efficient heat dissipation of the components. The temperature of the target components can reach about 25 °C [17]. To control the temperature of the primary mirror within the target temperature range, a highly thermally conductive graphite membrane is made into a special sheet as shown in Fig. 4. The membrane is adhered to the back and ribs of the primary mirror. Moreover, the edge of the graphite membrane is extended and adhered to the surface of the Invar annular bracket outside the piezoelectric actuator using silicon rubber. The Invar annular bracket and the main frame ($\leq 25 \pm 1$ °C) are also thermally installed. Part of the energy incident from the sun is transmitted to the back of the primary mirror through the front mirror surface, and then the membrane on the back of the mirror conducts the heat of the mirror to the surface of the Invar annular bracket outside the piezoelectric actuator. The heat is finally transmitted through the Invar annular bracket to the main frame. Another part of the energy incident from the sun is transmitted to the piezoelectric actuator through the transition ring of the primary mirror. The piezoelectric actuator is thermally connected to the aluminum bracket, and the heat is conducted to the bottom frame through the aluminum bracket for heat dissipation. Fig. 5 shows the location and heat flow diagram of the membrane.

3. Theoretical analysis of the thermal transfer of the primary mirror

3.1. Modeling

This section establishes a theoretical thermal model. We analyze and calculate the temperature distribution of the LST primary mirror in high-temperature observation mode in the space environment. The analysis includes the satellite flight attitude and orbital parameters, internal heat source input, and external temperature constraints. The working conditions are that the primary mirror is

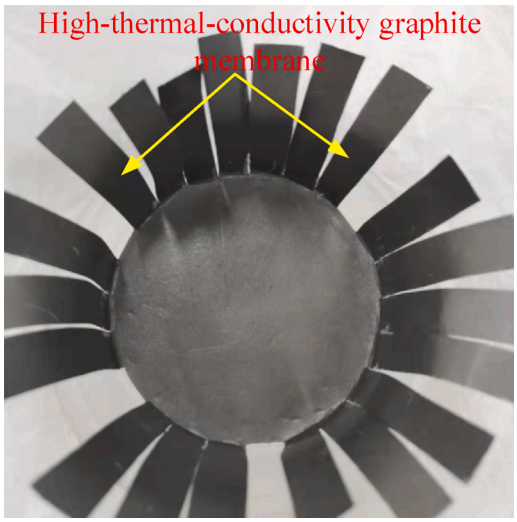

Fig. 4. Cutting shape of graphite membrane with high thermal conductivity.

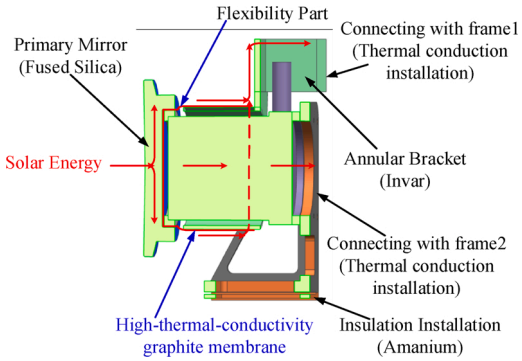

Fig. 5. Position and heat flow diagram of graphite membrane.

always oriented toward the sun, the external heat flow is maximum, the solar constant is 1412 W/m^2, the internal power consumption is the highest expected, and the thermal control coating is the end-of-life value. We determine whether the primary mirror meets the corresponding thermal control target in this working mode. A finite element network model is set up for the LST main mirror in the following steps: [18–21]

(1) Transient heat transfer differential equations

The transient temperature field equation for constant properties is

$$\rho c\frac{\partial T}{\partial t}=k(\frac{\partial^2 T}{\partial^2 x^2}+\frac{\partial^2 T}{\partial^2 y^2}+\frac{\partial^2 T}{\partial^2 z^2})+\Phi \tag{1}$$

where ρ is the material density, c is the material heat capacity, and t is the time. After finite element spatial dispersion, the transient heat conduction equation is

$$\boldsymbol{K}\cdot\boldsymbol{T}+\boldsymbol{C}\frac{\partial T}{\partial t}=\boldsymbol{P}, \tag{2}$$

where $\boldsymbol{C}$ is the heat capacity matrix, and $\frac{\partial T}{\partial t}$ is the derivative matrix of the node temperature versus time. The backward difference of (2) is

$$(\boldsymbol{K}+\frac{\boldsymbol{C}}{\Delta T})\cdot\boldsymbol{T}_t=\frac{\boldsymbol{C}}{\Delta t}\cdot\boldsymbol{T}_{t-\Delta t}+\boldsymbol{P}_t \tag{3}$$

Through the above formula, the temperature matrix $\boldsymbol{T}$ of the node is calculated iteratively.

(2) Boundary conditions

The initial temperature conditions and thermal boundary conditions are

$$T(x,y,z)|_{t=0}=T_0(x,y,z), \tag{4}$$

$$T(x,y,z)|_S=T_W(x,y,z), \tag{5}$$

$$\kappa_n\frac{\partial T}{\partial n}\Big|_{S_c}=-q(x,y,z), \tag{6}$$

$$\kappa_n\frac{\partial T}{\partial n}\Big|_{S_\varepsilon}=\sigma_\varepsilon(T^4-T_E^4), \tag{7}$$

where T_0 is the initial temperature, T_W is the temperature at a given boundary condition, T_E is the ambient temperature, S_c is the thermal boundary, S_ε is the radiation boundary, n is the direction of the boundary normal, q is the thermal flow intensity of the component surface, σ_ε is the Stefan-Boltzmann constant, and ε is the emissivity of the component surface.

(3) Establishing the thermal model of the primary mirror

A finite element network model of the LST primary mirror is established using the thermal analysis model. The mirror grid model is shown in Fig. 6. The thermal analysis model is divided into 7930 units and 4698 nodes, and 10 pairs of thermal couplings are

established.

To sum up, Eqs. (1) to (7) can be applied according to each unit, node, and coupling relationship in the model using the satellite flight attitude and orbital parameters, internal heat source input, external temperature constraints, operating conditions, and other requirements. We use the finite element method [22–26] to solve the temperature field equations simultaneously and obtain the temperature data of each characteristic point.

3.2. Parameters of finite element analysis

Table 1 shows the material properties of the primary mirror relevant to the analysis model derived above, and Table 2 shows the parameters of the highly thermally conductive graphite membrane. The temperature boundary is calculated via thermal analysis in high-temperature operating mode to obtain the temperature distribution of each characteristic point of the primary mirror. To simulate the temperature distribution of the primary mirror in this mode, the mirror is always oriented toward the sun when it is in orbit. The LST primary mirror is in a 4 K vacuum environment as a whole. The thermal load in the center area of the primary mirror is 2 W. The temperature boundary of the piezoelectric actuator bracket is 25 °C. The thermal resistance between the internal membrane and the actuator bracket is 0.28 °C/W, the thermal resistance between the external membrane and the actuator bracket is 0.25 °C/W, and the thermal resistance between the mirror rib and the front of the membrane is 0.43 °C/W. Table 3 shows the contact coefficients and thermal resistance parameters of the LST primary mirror. We simulate a working time of 15,000 s under high temperature and calculate the temperature distribution of the primary mirror when the temperature is stable.

4. Experimental verification

To verify the thermal design and the feasibility of the thermal control measures of the primary mirror, we obtained the temperature distribution of each characteristic point of the primary mirror in high-temperature operating mode. We performed a thermal equilibrium test on the appraisal component of the LST primary mirror. The test device and test platform are shown in Fig. 7. The test platform of the primary mirror simulated the space environment in a 1.5 m vacuum tank. The heat absorption of the primary mirror was simulated by a heating sheet. A layer of polyimide tape was pasted on the mirror surface to reduce the effect of the heating sheet on it. The heating sheet was attached to the outer surface of the polyimide tape and pasted in the center of the primary mirror. The size of the heating sheet was Φ 70 mm, the resistance was 11 Ω, and the current was set to 0.42 A. More than 90 % of the heat absorbed by the primary mirror was guided to the frame through the annular bracket. The primary mirror's external radiation heat dissipation was ≤10 %. The boundary simulation scheme was as follows:

(1) 300 mm × 300 mm heat sink was used to simulate the heat sink of the primary mirror assembly, and the material was aluminum alloy.
(2) An active temperature control circuit was set on the surface of the heat sink. The size of the heating sheet was 100 mm × 50 mm, the resistance was 98 Ω, the current was set to 0.15 A, and the temperature control target was 25 °C. A

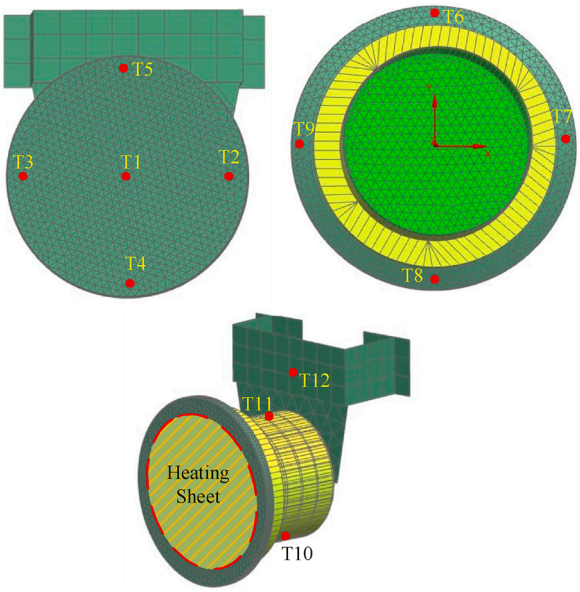

Fig. 6. Finite element network model of LST primary mirror and specific position of temperature control sensor.

Table 1
Material properties of primary mirror.

Material	Coating	Thermal conductivity (W/m/°C)	Coefficient of linear expansion /°C (60~120℃)	Density (kg/m^3)	Specific heat capacity(J/kg°C)
Fused silica	Mo/Si	1.38	2.1e-7	2200	787

Table 2
Material properties of high-thermal-conductivity graphite membrane.

Num.	Material properties	Value
1	Thermal conductivity in XY plane direction (W/m·K)	1200
2	Z direction thermal conductivity (W/m·K)	5
3	Density (g/cm^3)	2
4	Coefficient of linear expansion 10^{-6} (288K~1273 K)	1.5
5	Tensile strength (MPa)	12

Table 3
Contact coefficients and thermal resistance parameters of the LST primary mirror.

Connection relationship between the primary mirror components		Processing method of installation interface	Contact coefficient (W/(m^2 K)	Contact thermal resistance (°C/W)
Component 1	Component 2			
Primary mirror	Transition ring	Three-point contact (silicone)	200	104.20
Transition ring	Piezoelectric actuator	Ring contact (silicone)	200	5.15
Annular bracket	Main frame	Filled indium foil	2000	0.25
Piezoelectric actuator	Aluminum bracket	Only metal contact	200	1.47
Aluminum bracket	Insulation pads	Only metal contact	200	3.85
Insulation pads	Bottom frame	Only metal contact	200	3.70
Primary mirror back	Inner graphite membrane	Silicone	1000	0.34
Inner graphite membrane	Annular bracket	Silicone	1000	0.13
Primary mirror rib	External graphite membrane	Silicone	1000	0.33
External graphite membrane	Annular bracket	Silicone	1000	0.14

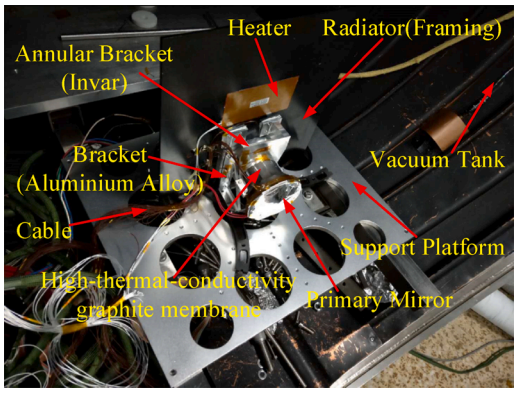

Fig. 7. Thermal equilibrium test device and platform for appraisal component of the LST primary mirror.

thermocouple was used to monitor the temperature. Table 4 shows the sensor planning for the heat equilibrium test of the primary mirror, and Fig. 6 marks the site of the heating sheet and the position of the temperature control sensor.

(3) The radiation environment of the primary mirror component was replaced by a vacuum tank, which requires a heat sink temperature of 18–22 °C.

(4) The purpose of this test was to verify the effectiveness of heat conduction and heat dissipation. A 20-unit multilayer thermal insulation component was pasted on the primary mirror to reduce the influence of the heat dissipation uncertainty of the primary mirror on the test data. The mask consisted of a double-sided aluminized polyester membrane.

Finally, the temperature fluctuation on the back of the main mirror was no more than ±0.5 °C, or the monotone value was less than

Table 4
Thermal equilibrium test sensor list of primary mirror.

Num.	Sensor code	Position
1	T1	Primary mirror front, heating sheet center
2	T2	Primary mirror front -Y
3	T3	Primary mirror front + Y
4	T4	Primary mirror front + Z
5	T5	Primary mirror front -Z
6	T6	Primary mirror back -Z
7	T7	Primary mirror back + Y
8	T8	Primary mirror back + Z
9	T9	Primary mirror back -Y
10	T10	Annular bracket -Z
11	T11	Annular bracket + Z
12	T12	Aluminum frame + Z

0.1 °C /h in the heat equilibrium test for 4 h continuously, to judge the balance condition of the test.

5. Absolute power: comparison between theoretical and experimental results

The simulation results show that the temperature of the center of the primary mirror is 38.98 °C, the temperature in the + Y direction of the mirror is 31.51 °C, the temperature in its –Y direction is 31.42 °C, and the temperature in its + Z direction is 31.16 °C. The average temperature of the mirror is 31.36 °C. In the thermal equilibrium test of the appraisal component of the primary mirror, the temperature of the mirror center is 38.88 °C, the temperature in the + Y direction of the mirror is 31.21 °C, the temperature in its –Y direction is 31.64 °C, and the temperature in its + Z direction is 31.59 °C. The average temperature of the primary mirror is 31.56 °C, and Fig. 8 shows the comparison between the simulated and experimental temperatures of the mirror front.

The finite element network simulation results are as follows: the temperature in the + Y direction of the mirror back was 31.55 °C, the temperature in the –Y direction of the mirror back was 30.21 °C, the temperature in the + Z direction of the mirror back was 30.12 °C, and the average mirror temperature was 30.63 °C. The thermal equilibrium test results for the appraisal component of the primary mirror are as follows: the temperature in the + Y direction of the mirror back was 30.97 °C, the temperature in the + Y direction of the mirror back was 29.27 °C, the temperature in the + Z direction of the mirror back was 29.56 °C, and the average mirror temperature was 30.01 °C. Fig. 9 shows the comparison between the simulated and experimental temperatures of the primary mirror back.

The temperature comparison curves of the finite element network simulation and thermal equilibrium test show the following: the overall temperature of the primary mirror is unevenly distributed, and its center temperature is relatively high. The temperature gradually stabilizes within the operating time of 15,000 s and does not exceed the thermal control target of 40 °C. The temperature difference between the simulation and experiment is only 0.1 °C. Because the graphite membrane conducts the central heat of the mirror to the main frame through the mirror back, the circumferential temperature of the primary mirror is lower than the center temperature, and both are <32 °C. The radial temperature difference of the mirror is large, and the circumferential temperature difference is small. The finite element simulation and thermal equilibrium test have basically the same temperature trend at each point. The thermal conductivity of the membrane on the ribs makes the overall temperature of the back of the mirror lower than the temperature of the mirror surface, and the temperature difference is small. The finite-element-simulated temperature of the back of the

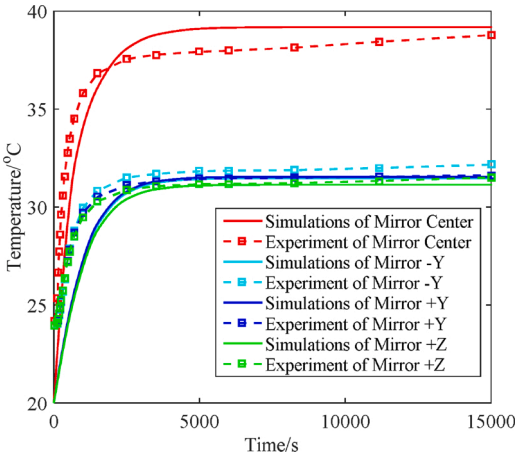

Fig. 8. Comparison of simulated and experimental temperatures of primary mirror front.

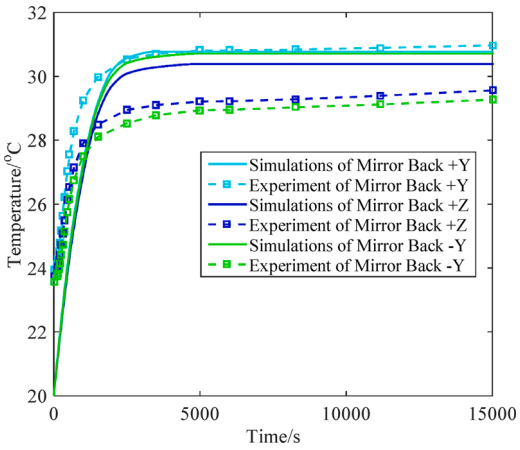

Fig. 9. Comparison of simulated and experimental temperatures of primary mirror back.

mirror is higher than in the heat equilibrium test, with a maximum temperature difference of < 1 °C. To sum up, the simulation results in the finite element network model are basically consistent with the thermal equilibrium test results. The temperature of each part of the primary mirror is stable in high-temperature operating mode and meets the requirements of the thermal control target. Therefore, using the graphite membrane with the primary mirror is feasible, meets the theoretical thermal control requirements, and maintains good temperature stability. Table 5 shows the temperature comparison between the thermal equilibrium test and the finite element network simulation.

6. Results of LST orbital simulation

The primary mirror assembly was mounted into the entire LST model, and an orbital simulation was performed using the finite element network model. In high- and low-temperature observation, we verified that the LST primary mirror satisfies the thermal control target of <40 °C when operating at 720 km in a sun-synchronous orbit.

In high-temperature observation mode, the LST primary mirror is always oriented directly toward the sun. Fig. 10 shows the cloud diagram of the simulated temperature distribution between the front and the back of the primary mirror for high-temperature orbital observation assuming the maximum external heat flux, a solar constant of 1412 W/m^2, the maximum expected internal power consumption, and the end-of-life thermal control coating (solar absorptivity $\alpha_s = 0.42$, emission $\varepsilon = 0.30$). The maximum temperature in the center of the primary mirror is 38.48 °C, the average temperature in the circumferential direction is 32.36 °C, and the average backside temperature of the mirror is 30.35 °C.

In low-temperature observation mode, the primary mirror is always oriented directly toward the sun. Fig. 11 shows the cloud diagram of the simulated temperature distribution between the front and the back of the primary mirror for low-temperature orbital observation assuming the minimum external heat flux, a solar constant of 1322 W/m^2, the minimum expected internal power consumption, and the initial-life thermal control coating ($\alpha_s = 0.38$, $\varepsilon = 0.41$). The maximum temperature in the center of the primary mirror is 33.96 °C, the average temperature in the circumferential direction is 30.93 °C, and the average temperature in the back circumferential direction is 29.32 °C.

The information above is used to analyze the LST machine model via the finite element network orbital simulation. The temperature of each characteristic point of the primary mirror meets the thermal control target (<40 °C). Fig. 12a shows the temperature distribution at the center of the mirror, in the circumferential direction of the mirror, and in the circumferential direction of the back of the mirror under high temperature; Fig. 12b presents the corresponding low-temperature distributions. Table 6 summarizes the high- and low-temperature distribution data of the orbiting primary mirror assembly.

7. Conclusion

We studied the thermal design of a high-thermal-conductivity graphite membrane applied to the LST primary mirror and conducted a finite element network simulation and thermal equilibrium test. The following are the principal findings and conclusions:

(1) The membrane effectively reduces the temperature due to direct radiation from the sun to the primary mirror, and solves the problems of the high heat absorption of the mirror, its uneven temperature distribution, and its need for continuous high-frequency image stabilization for thermal control.
(2) A finite element network simulation under high temperature showed that the circumferential temperature of the primary mirror was significantly lower than the center temperature, and the maximum temperature at the mirror center met the thermal control target of <40 °C.

Table 5
Comparison of characteristic temperatures of primary mirror obtained via thermal equilibrium test and simulation of finite element network model.

Position	Thermal equilibrium test temperature (°C)	Finite element network model simulation temperature (°C)	Temperature difference (°C)
Primary mirror center	38.88	38.98	0.10
Primary mirror front + Y	31.21	31.51	0.30
Primary mirror front -Y	31.64	31.42	0.22
Primary mirror front + Z	31.59	31.16	0.43
Primary mirror back + Y	30.97	31.55	0.58
Primary mirror back -Y	29.27	30.21	0.94
Primary mirror back + Z	29.56	30.12	0.56
Annular bracket	29.12	29.57	0.43

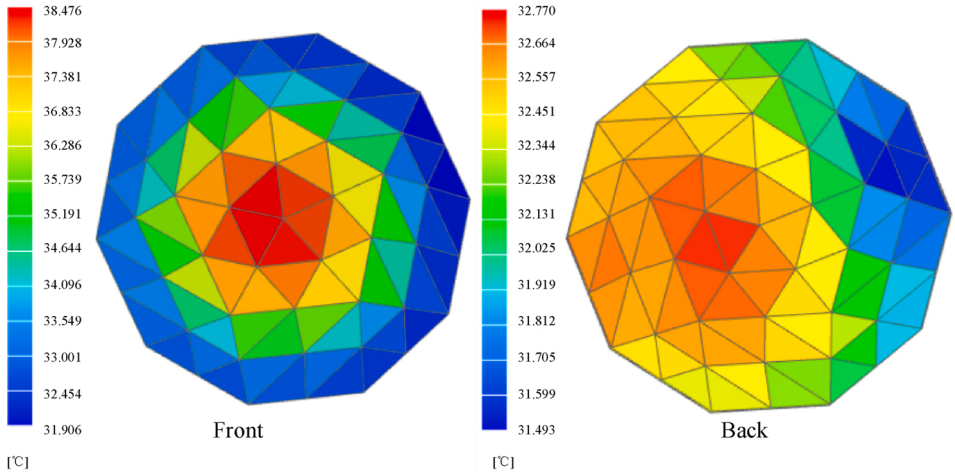

Fig. 10. Cloud diagram of high-temperature distribution of the front and back of the primary mirror.

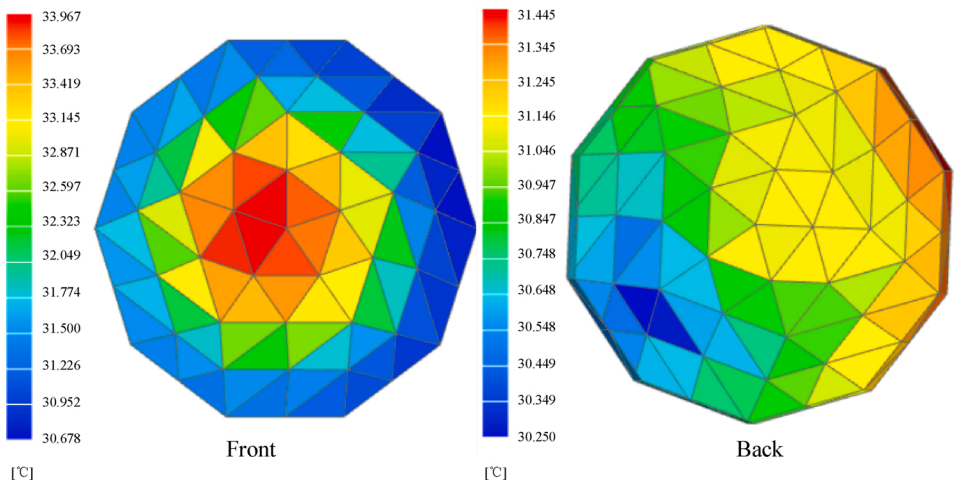

Fig. 11. Cloud diagram of low-temperature distribution of the front and back of the primary mirror.

(3) The temperature distribution of each characteristic point of the primary mirror was obtained through a thermal equilibrium test. The temperature variation in this test was consistent with that in the simulation, which verified the appropriateness of the thermal design.

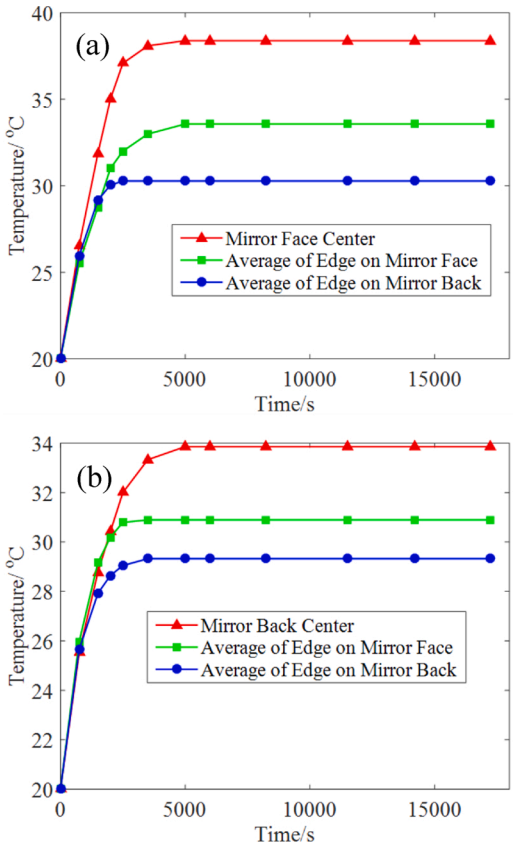

Fig. 12. Average temperature distribution of primary mirror center, circumferential direction of mirror surface, and circumferential direction of mirror back under (a) high and (b) low temperatures.

Table 6
emperature distribution of the primary mirror assembly under high and low temperatures in orbit.

Observation mode /Position/AVE. temperature (°C)	High temperature observation	Low temperature observation
Primary mirror center	38.48	33.96
Primary mirror front	32.36	30.93
Primary mirror back	30.35	29.32

(4) An orbital simulation of an entire LST model in high- and low-temperature observation showed that the temperature of each characteristic point of the primary mirror satisfies the corresponding thermal control target (<40 °C) in both working conditions.
(5) The temperature of the primary mirror in the orbital simulation of both LST working modes is highly consistent with that in the thermal equilibrium test. The temperature distribution is stable, and the primary mirror works normally and efficiently.

Funding

This research was funded by the National Natural Science Foundation of China, grant number 61605203, and Advanced Space-based Solar Observatory (ASO-S) satellite, grant number XDA15320000.

Declaration of Competing Interest

The authors declare no conflict of interest.

Acknowledgements

Mark Kurban from Liwen Bianji, Edanz Editing China (www.liwenbianji.cn/ac), edited a draft of this manuscript.

References

[1] J. Schou, P.H. Scherrer, R.I. Bush, R. Wachter, S. Couvidat, M.C. Rabello-Soares, et al., Design and ground calibration of the helioseismic and magnetic imager (HMI) instrument on the solar dynamics observatory (SDO), Solar Phys. 275 (2012) 229–259.
[2] C. Zheng, J.H. Qi, J. Fu, J.W. Song, L. Cheng, Thermal analysis on Alpha Magnetic Spectrometer main radiators under the flight attitude adjustment of International Space Station, Appl. Therm. Eng. 164 (2020) 561–572.
[3] Y. Suematsu, S. Tsuneta, K. Ichimoto, T. Shimizu, M. Otsubo, Y. Katsukawa, et al., The solar optical telescope of Solar-B (Hinode): the optical telescope assembly, Solar Phys. 249 (2008) 197–220.
[4] M. Tumarina, M. Ryazanskiy, S. Jeong, G. Hong, N. Vedenkin, I.H. Park, A. Milov, Design, fabrication and space suitability tests of wide field of view, ultra-compact, and high resolution telescope for space application, Opt. Express 26 (2018) 2390–2399.
[5] Y. Suematsu, Y. Katsukawa, T. Shimizu, K. Ichimoto, T. Horiuchi, Y. Matsumoto, et al., Short telescope design of 1.5-m aperture solar UV visible and IR telescope aboard Solar-C, Sol. Phys. Spac. Wea. Instr. 8148 (2011).
[6] C.M. Pieters, J. Boardman, B. Buratti, A. Chatterjee, R. Clark, T. Glavich, et al., The moon mineralogy mapper (M-3) on Chandrayaan-1, Current Sci. 96 (2009) 500–505.
[7] P. Cheimets, D.C. Caldwell, C. Chou, R. Gates, J. Lemen, W.A. Podgorski, et al., SDO-AiA telescope design, Int. Soc. Opt. Eng. 7438 (2009) 12–25.
[8] T.N. Woods, F.G. Eparvier, R. Hock, A.R. Jones, D. Woodraska, D. Judge, et al., Extreme ultraviolet variability experiment (EVE) on the solar dynamics observatory (SDO): overview of science objectives, instrument design, data products, and model developments, Solar Phys. 275 (2012) 115–143.
[9] L. Han, P. Krstic, I. Kaganovich, R. Car, Migration of a carbon adatom on a charged single-walled carbon nanotube, Carbon 116 (2017) 174–180.
[10] M.H. Jalaei, A.G. Arani, H. Tourang, On the dynamic stability of viscoelastic graphene sheets, Int. J. Eng. Sci. 132 (2018) 16–29.
[11] R. Al-Shannaq, M.M. Farid, A novel graphite-PCM composite sphere with enhanced thermo-physical properties, Appl. Therm. Eng. 142 (2018) 401–409.
[12] G. Liu, L. Guo, R.C. Hu, Q.W. Wu, Space camera carbon Fiber truss thermal design, Opt. Precision Eng. 25 (2017) 2405–2412 (in Chinese).
[13] A. Mazloum, V. Oddone, S. Reich, I. Sevostianov, Connection between strength and thermal conductivity of metal matrix composites with uniform distribution of graphite flakes, Int. J. Eng. Sci. 139 (2019) 70–82.
[14] M. Joseph, V. Sajith, Graphene enhanced paraffin nanocomposite based hybrid cooling system for thermal management of electronics, Appl. Therm. Eng. 163 (2019) 712–716.
[15] M. Carmona, E. Perez, M. Palacio, Experimental evaluation of porosity, axial and radial thermal conductivity, of an adsorbent material composed by mixture of activated carbon, expanded graphite and lithium chloride, Appl. Therm. Eng. 150 (2019) 456–463.
[16] Y. Li, Q.W. Wu, L.H. Chen, Y. Huang, H.W. Liu, Thermal control system for carbon dioxide detector, Opt. Precision Eng. 23 (2015) 1053–1061 (in Chinese).
[17] C.C. Shen, M.M.A. Green, O.O. Breitenstein, T.T. Trupke, M. Zhang, H. Kampwerth, Solar energy materials and solar cells, Sol. Energy Mater. Sol. Cells 116 (2009) 262.
[18] T.W. Q, Numerical Heat Transfer, second ed., Xi'an Jiao Tong University Press, Xi'an, 2001.
[19] T.W.Q. Yang, M. Sh, Heat Transfer, second ed., Higher Education Press, Beijing, 1998.
[20] H.J. P, Heat Transfer, China Machine Press, Beijing, 2005.
[21] R.J. Wang, Y.H. Pan, Y.L. Nian, W.L. Cheng, Study on dynamic thermal control performance of positive temperature coefficient (PTC) material based on a novel heat transfer model considering internal heat transfer, Appl. Therm. Eng. 165 (2020) 336–352.
[22] W. Yang, M. Shi, Study on heat transfer model of vertical u tube ground heat exchangers based on line heat source theory, Acta. Energiae Sol. Sinica. 28 (2007) 482–488.
[23] S. Li, L. Chen, Y. Yang, Thermal design and test verification of the solar X-Ray and extreme ultraviolet imager, Optik 203 (2020) 32–42.
[24] S.P. Parida, P.C. Jena, R.R. Dash, FGM beam analysis in dynamical and thermal surroundings using finite element method, Mater. Today. 18 (2019) 3676–3682.
[25] Z. She, K. Wang, H. Liu, Thermal analysis of elliptical fiber-reinforced composites by the hybrid Trefftz finite element method, Int. J. Heat Mass Transfer. 144 (2019) 356–367.
[26] E. Soylemez, High deposition rate approach of selective laser melting through defocused single bead experiments and thermal finite element analysis for Ti-6Al-4V, Additive Manuf. 31 (2020) 215–226.